Nonlinear dynamics of the polarization of multitransverse mode vertical-cavity surface-emitting lasers under current modulation

A. Valle,[1,*] M. Sciamanna,[2] and K. Panajotov[3,4]
[1]*Instituto de Física de Cantabria, CSIC-Universidad de Cantabria, Avda. Los Castros s/n, E-39005, Santander, Spain*
[2]*Supélec, Laboratoire Matériaux Optiques, Photonique et Systèmes (LMOPS), CNRS UMR-7132, F-57070, Metz, France*
[3]*Department of Applied Physics and Photonics (TW-TONA), Vrije Universiteit Brussels, B-1050 Brussels, Belgium*
[4]*Institute of Solid State Physics, 72 Tzarigradsko Chaussee Boulevard, 1784 Sofia, Bulgaria*
(Received 25 April 2007; published 4 October 2007)

In this paper we report on a theoretical investigation of the nonlinear dynamics of the polarization of multitransverse mode vertical-cavity surface-emitting lasers (VCSELs) under current modulation. Special attention is given to the comparison with a previously studied case of single-transverse mode VCSEL emitting in two orthogonal polarizations. The consideration of spatial effects in VCSEL modifies the polarization dynamics that accompanies the period doubling route to chaos for large modulation amplitudes. Depending on the modulation parameters, the excitation of a higher order transverse mode may either induce chaotic pulsing in an otherwise regularly pulsating VCSEL, or induce a time-periodic pulsing dynamics in an otherwise chaotic VCSEL. Bifurcation diagrams obtained for different modulation frequencies, several values of the dichroism, and different transverse mode characteristics allow us to identify the different scenarios of polarization dynamics in a directly modulated VCSEL. Temporal analysis of carrier number radial profile reveals considerable changes for the multitransverse mode case only constituting the physical origin of the reported changes in the temporal and polarization dynamics.

DOI: 10.1103/PhysRevE.76.046206 PACS number(s): 05.45.−a, 42.55.Px, 42.65.Sf

I. INTRODUCTION

Semiconductor lasers can be divided in two main categories depending on the dimensions and the geometry of the active cavity: edge-emitting lasers (EELs) and vertical-cavity surface-emitting lasers (VCSELs). VCSELs present significant advantages over their edge-emitting counterparts, including low threshold current, low cost, circular output beam, and easy fabrication in two-dimensional arrays. Although VCSELs are intrinsically single-longitudinal mode devices, emission in multiple transverse and polarization modes is usually found [1]. The polarization is not well fixed and small changes of the injection current or the device temperature may result in a polarization switching (PS) between the two linearly polarized modes. While emission in several transverse modes is usually attributed to spatial-hole burning effects [2–4], a number of different physical mechanisms can be responsible for PS phenomenon in VCSELs. Therefore, different models of PS in VCSELs have been suggested, for example, those taking into account spin relaxation mechanisms in semiconductor quantum wells (spin flip model, SFM) [5,6], thermal effects [7], or the relative modification of the net modal gain and losses with the injection current [8–10].

The dynamics of directly modulated semiconductor lasers has been studied for more than twenty years. Depending on the modulation parameters (modulation depth and modulation amplitude), but also on the laser internal parameters, the laser may exhibit ultrafast sharp pulses in the emitted power but also complex time-dependent dynamics such as period doubling and possibly chaotic pulsating behavior [11–20]. Most of the existing studies relate to conventional EELs [11–16]. Studies of nonlinear dynamics in directly modulated VCSELs remain scarce [17–20], while being of great interest both for fundamental and applied research [21]. Nonlinear dynamics has been theoretically analyzed for linearly polarized single-transverse mode [17,18] and multimode VCSELs [18,19]. Chaotic behavior appears in the multimode regime due to transverse mode competition [18,19]. Also, the nonlinear dynamics of the two orthogonal polarizations of a directly modulated single-transverse mode VCSEL has been studied [20]. Chaotic dynamics due to polarization competition has been found in a large range of laser and modulation parameters [20]. The chaotic dynamics of the polarization is found for much smaller amplitudes and frequencies of modulation than the chaotic dynamics of the transverse modes of the VCSEL. This occurs since the differences in gain or loss between the two polarizations of a given transverse mode are much smaller than gain or loss differences between different transverse modes [20] and then stronger competition between the orthogonal polarizations is obtained.

In this paper we generalize those previous studies by analyzing the dynamical behavior of the polarization of a multitransverse mode VCSEL subject to current modulation. Our theoretical study is based on a model that takes into account polarization and spatial effects. We first analyze the case of a single-transverse mode VCSEL. We study the role played by the spatial effects by comparing with results obtained by using a spatially independent description of that system. The inclusion of the spatial effects leads to the appearance of new polarization dynamics. In the second part of our work we focus on the multitransverse mode VCSEL. Chaotic regimes that involve several polarized transverse modes are found in a large range of parameters. Special attention is given to the comparison with the case of a single-transverse mode VC-

*FAX: 34 942 200935; valle@ifca.unican.es

SEL emitted in two orthogonal polarizations for a better understanding of the effect of the additional higher-order transverse mode in the dynamics. The range of modulation amplitudes in which we obtain complex dynamics is larger than for the single-transverse mode case. However, situations in which the addition of the higher-order mode leads to simpler dynamics are also found.

Our paper is organized as follows. In Sec. II the theoretical model is presented. In Sec. III we present our results corresponding to the role played by the spatial effects on the polarization of the single-transverse mode VCSEL. In Sec. IV we analyze the nonlinear dynamics of the polarization of the multimode VCSEL. Finally, in Sec. V a brief discussion and a summary of our results are presented.

II. MODEL

In this work we consider a model of a multitransverse mode VCSEL [22–24] that takes into account two of the mechanisms that can define the polarization of the laser. The first one is associated with the combined effect of the VCSEL anisotropies, the linewidth enhancement factor, and the spin-flip relaxation processes within a framework known as the SFM model [5]. The second mechanism is related to the effect of having different electrical field profiles for each linear polarization due to the birefringence of the device [9]. We consider cylindrically symmetric weak index-guided devices with the structure illustrated in the Fig. 1 of Ref. [24]. The radius of the core region and the length of the cavity are denoted as a and L, respectively. Subscripts x and y will be used to denote the polarization direction. Birefringency is taken into account by assuming that the core refractive index in the x direction, $n_{core,x}$, is larger than in the y direction, $n_{core,y}$—hence the x polarized mode emission frequency is lower than that of the y polarized mode—while the cladding refractive index, n_{cladd}, is the same in both directions. We will consider a small value of the index step (0.005) in such a way that the appropriate transverse modes of the structure are the linearly polarized modes of mn order, LP_{mn}. That index step we consider is much greater than the contribution due to the carrier-induced refractive index and then the evolution obtained with our model, based on a modal expansion, would coincide with the one obtained with a full spatiotemporal model [25]. Here we treat the case of VCSELs that can operate in the fundamental (LP_{01}) and in the first order (LP_{11}) transverse modes. Subscripts 0,1 will be used to denote the LP_{01} and LP_{11} modes, respectively. In the basis of the linearly polarized modes and considering radial symmetry of the cavity the optical field can be written as [22–24]

$$\vec{E}(r,t) = [(E_{0x}(t)\psi_{0x}(r) + E_{1x}(t)\psi_{1x}(r))\vec{x} + (E_{0y}(t)\psi_{0y}(r) + E_{1y}(t)\psi_{1y}(r))\vec{y}]e^{i\kappa\alpha t} + \text{c.c.}, \quad (1)$$

where ψ_{0j} and ψ_{1j} are the modal profiles of the LP_{01} and LP_{11} modes, respectively, obtained by solving the Helmholtz equation [9]; E_{0j} and E_{1j} are the modal amplitudes of these modes, the subindex j stands for the linear polarization state of the given mode; κ is the electric field decay rate that includes the internal and facet losses, and α is the alpha factor or linewidth enhancement factor that describes phase-amplitude coupling mechanisms in semiconductor lasers. The equations that describe the polarization and transverse mode behavior of the VCSEL, written appropriately in the cylindrical basis, read [24]

$$\dot{E}_{0x} = \kappa(1+i\alpha)[E_{0x}(g_{0x}-1) + iE_{0y}g_{0xy}] - (\gamma_a + i\gamma_{p0})E_{0x},$$

$$\dot{E}_{0y} = \kappa(1+i\alpha)[E_{0y}(g_{0y}-1) - iE_{0x}g_{0yx}] + (\gamma_a + i\gamma_{p0})E_{0y},$$

$$\dot{E}_{1x} = \kappa(1+i\alpha)[E_{1x}(g_{1x}-\kappa_r) + iE_{1y}g_{1xy}] + i\gamma_p^{tr}E_{1x} - (\gamma_a + i\gamma_{p1})E_{1x},$$

$$\dot{E}_{1y} = \kappa(1+i\alpha)[E_{1y}(g_{1y}-\kappa_r) - iE_{1x}g_{1yx}] + i\gamma_p^{tr}E_{1y} + (\gamma_a + i\gamma_{p1})E_{1y},$$

$$\frac{\partial N(r,t)}{\partial t} = D\nabla_\perp^2 N - \gamma_e\left[N\left(1 + \sum_{i=0,1}\sum_{j=x,y}|E_{ij}|^2\psi_{ij}^2(r)\right) - \mu(t)C(r) - in\sum_{i=0,1}(E_{ix}E_{iy}^* - E_{iy}E_{ix}^*)\psi_{ix}(r)\psi_{iy}(r)\right],$$

$$\frac{\partial n(r,t)}{\partial t} = -\gamma_s n + D\nabla_\perp^2 n - \gamma_e\left[n\sum_{i=0,1}\sum_{j=x,y}|E_{ij}|^2\psi_{ij}^2(r) - iN\sum_{i=0,1}(E_{ix}E_{iy}^* - E_{iy}E_{ix}^*)\psi_{ix}(r)\psi_{iy}(r)\right], \quad (2)$$

where $N(r,t)$ is the total carrier number and $n(r,t)$ is the difference in the carrier numbers of the two magnetic sublevels. The possibility of having an external gain-loss anisotropy for both polarizations is considered through the dichroism, γ_a, parameter. The possibility of having different losses for both transverse modes is also considered by taking into account the κ_r parameter, which is the relative loss of the LP_{11} mode with respect to the LP_{01} mode. The frequency splitting between the orthogonal polarizations of the LP_{01} mode, $2\gamma_{p0}/(2\pi)$, between the orthogonal polarizations of the LP_{11} mode, $2\gamma_{p1}/(2\pi)$, and between the two transverse modes with the same polarization, $\gamma_p^{tr}/(2\pi)$, are obtained from the calculation of the waveguide modes via the Helmholtz equation. We have chosen the values of $n_{core,x}$, $n_{core,y}$, and n_{cladd} in such a way that $\gamma_{p0}=1\ \mathrm{ns}^{-1}$, a value that corresponds to the one used in Ref. [20]. The total injected current is uniformly distributed across a circular disk contact of radius denoted as s, and then $C(r)=1$ if $r<s$, and $C(r)=0$, elsewhere. The prefactor $\mu(t)$ allows for the generation of a sinusoidal current and then $\mu(t)=\mu_{dc}+\Delta\mu\sin(2\pi F_u t)$, where μ_{dc} is the dc bias injection current, $\Delta\mu$ is the modulation amplitude, and $F_u \equiv 1/T$ is the modulation frequency. The normal gain normalized to the threshold gain, $g_{ij}(i=0,1,j=x,y)$, is defined as

TABLE I. Values and definitions of various parameters.

Symbol	Value	Meaning of the symbol
a	3 μm	Radius of the core region
L	1 μm	Length of the cavity
$n_{core,x}$	3.5000035	Refractive index of the core in the x direction
$n_{core,y}$	3.5	Refractive index of the core in the y direction
n_{cladd}	3.495	Refractive index of the cladding region
k	300 ns^{-1}	Field decay rate
α	3	Linewidth enhancement factor
γ_e	1 ns^{-1}	Decay rate for the total carrier population
γ_s	50 ns^{-1}	Spin-flip relaxation rate
D	3 cm^2 s^{-1}	Diffusion coefficient

$$g_{ij} = \frac{\int_0^\infty N(r,t)\psi_{ij}^2(r)rdr}{\int_0^\infty \psi_{ij}^2(r)rdr}, \tag{3}$$

and g_{ijk} $(i=0,1;jk=xy,yx)$ is given by

$$g_{i,jk} = \frac{\int_0^\infty n(r,t)\psi_{ij}(r)\psi_{ik}(r)rdr}{\int_0^\infty \psi_{ij}^2(r)rdr}. \tag{4}$$

Note that the modal gains for the x and y polarizations are different due to the different optical mode profiles. However, we neglect the material gain difference since the frequency splitting is very small compared to the width of the gain curve. The rest of the parameters that appear in the equations are specified in the Table I. In the following section we will present the results obtained by integrating numerically the previous set of equations. Time and space integration steps of 0.01 ps and 0.12 microns, respectively, have been used. The boundary conditions for the carrier distribution are taken as $N(\infty,t)=0$, $n(\infty,t)=0$.

III. FUNDAMENTAL TRANSVERSE MODE OPERATION: COMPARISON WITH THE SPATIALLY INDEPENDENT MODEL

In this section we will study the nonlinear dynamics of the two orthogonal linearly polarized fundamental transverse modes of the VCSEL when subject to a sinusoidal modulation of the current. Our results are obtained with the model of the previous section with similar parameters to those used in Ref. [20] for allowing a direct comparison with the results obtained with a spatially independent model of a single-transverse mode VCSEL. First we present some results corresponding to the cw operation of the VCSEL. We show in Fig. 1(a) the transverse and polarization mode-resolved light-current characteristics of the VCSEL when the current injection is uniform over a disk of radius equal to the radius of the waveguide, i.e., $s=a=3$ μm. In that figure the intensities of the polarized transverse modes, $I_{ij}=|E_{ij}|^2$ (where $i=0,1$; $j=x,y$), are plotted as a function of the dc current $\mu_d c$. The threshold current μ_{th}, is slightly larger, 1.135, than in the spatially independent model, 1, because carriers can diffuse out of the active region in the spatially dependent model [4]. Emission above threshold is in the y polarization of the fundamental transverse mode, as in Ref. [20]. The inclusion of spatial-hole burning effects in our model is responsible for the excitation of the higher-order mode. The emission in that mode is also in the y polarization. Experimentally, the first order transverse mode often appears with linear polarization orthogonal to the fundamental mode [1]. In our model such a situation can be observed by choosing the γ_a and κ_r parameters; however, for comparison purposes we consider the parameters of Ref. [20]. Nonlinear dynamics of our system is

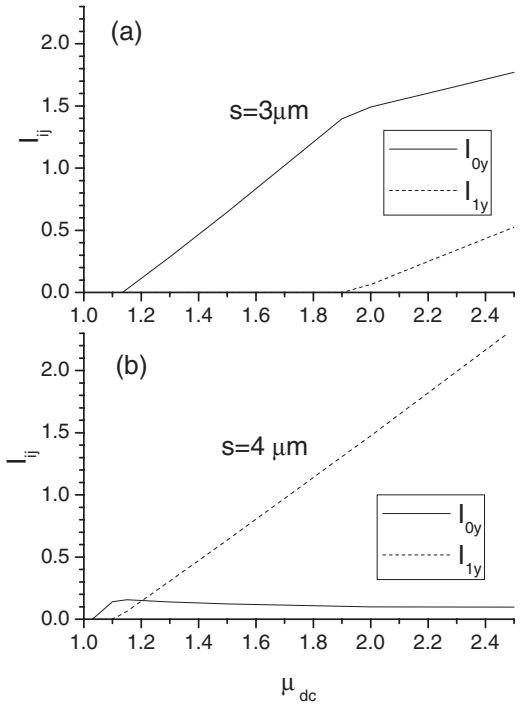

FIG. 1. Light-current characteristics of a VCSEL with a current injection region of (a) radius $s=3$ μm and (b) $s=4$ μm. Other parameters in this figure are $\gamma_a=0.1$ ns^{-1}, $\kappa_r=1$, and $\Delta\mu=0$.

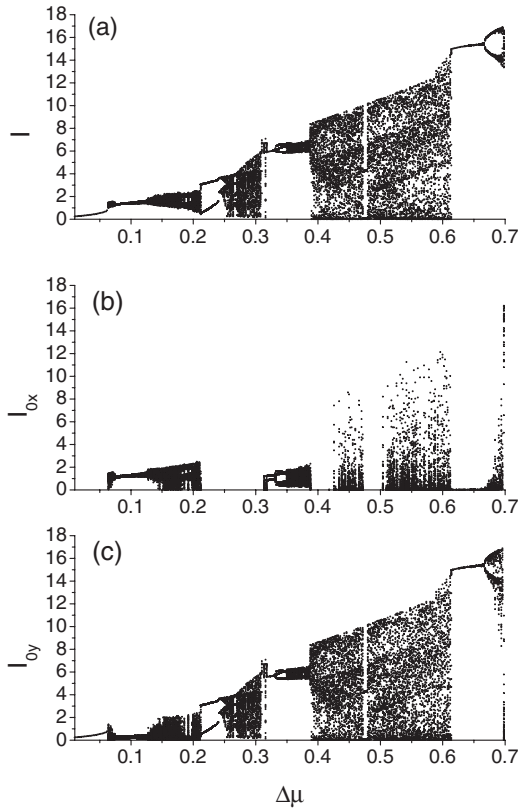

FIG. 2. Bifurcation diagrams of the (a) total, (b) $LP_{01,x}$, and (c) $LP_{01,y}$ intensities versus $\Delta\mu$, for $s=3$ μm, $F_u=1$ GHz, $\gamma_a=0.1$ ns^{-1}, $\mu_{dc}=1.1$ μ_{th}, and $\kappa_r=1$.

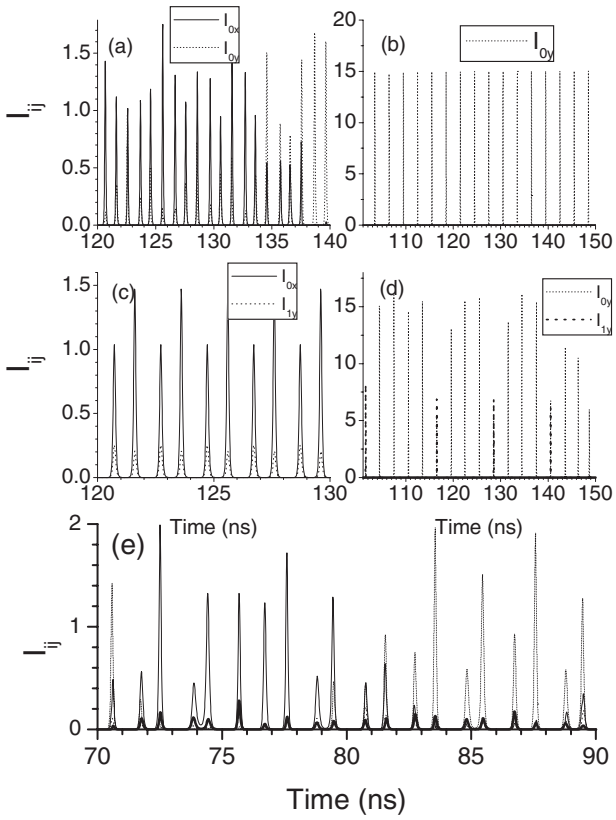

FIG. 3. Time traces of the intensities of the polarized transverse modes for specific values of $\Delta\mu$ (I_{0x}: solid thin line; I_{0y}: dotted thin line; I_{1x}: solid thick line; I_{1y}: dotted thick line). Results corresponding to Fig. 2 are plotted when (a) $\Delta\mu=0.14$ and (b) $\Delta\mu=0.62$. Results corresponding to Fig. 4 are plotted when (c) $\Delta\mu=0.14$, (d) $\Delta\mu=0.62$, and (e) $\Delta\mu=0.18$.

summarized by using bifurcation diagrams of the polarized transverse modes. These diagrams are calculated as follows. The bifurcation parameter $\Delta\mu$ is increased step by step. At each step $\Delta\mu$ is kept constant during 150 modulation periods. The initial conditions for the evolution at each value of $\Delta\mu$ are the final conditions that were obtained for the previous value of $\Delta\mu$. In this way bifurcation diagrams with a slow sweeping of the bifurcation parameter are obtained. The successive maxima of the intensities I_{ij} that appear in the last 100 modulation periods are then recorded for that $\Delta\mu$ value. Those maxima as a function of $\Delta\mu$ are the points that are represented in the bifurcation diagrams calculated in this work.

Our first bifurcation diagrams, shown in Fig. 2, are used to perform the comparison with the results of the polarization dynamics obtained with the spatially independent model of the single-transverse mode VCSEL of Ref. [20]. In Fig. 2 only the fundamental mode is excited since the range of modulation amplitudes has been chosen for not allowing the excitation of the LP_{11} mode. Figure 2(a) also shows the bifurcation diagram for the total intensity I. Similar dynamics to those observed in Fig. 1 of Ref. [20] are observed for values of $\Delta\mu$ smaller than 0.3. An example of those similar dynamics is found in Fig. 3(a) when $\Delta\mu=0.14$. The two polarizations exhibit chaoticlike dynamics with a fast modulation of their intensities at the modulation frequency in such a way that when one polarization fires a large pulse, the other polarization fires a small pulse. However, results differ from those of Ref. [20] when $\Delta\mu>0.3$. In the spatially independent model a period-doubling route to chaos is observed in the $LP_{01,y}$ mode with negligible values of the $LP_{01,x}$ intensity. When spatial effects are taken into account the $LP_{01,x}$ is also excited in such a way that the period-doubling route to chaos in the $LP_{01,y}$ mode is destroyed. Figure 2 also shows that chaotic excitation in both polarizations is found over wide $\Delta\mu$ windows if $\Delta\mu<0.61$. For larger values of $\Delta\mu$ time-periodic dynamics is again obtained. We show in Fig. 3(b) a typical time-periodic dynamics in which a $3T$-periodic response is observed for the $LP_{01,y}$ mode. The results of this section indicate that as the modulation amplitude increases the spatial effects become more relevant for describing the dynamics of the two orthogonal linearly polarized fundamental transverse modes: the inclusion of spatial effects leads to the excitation of the otherwise depressed x-LP fundamental transverse mode, which then competes with the y-LP fundamental transverse mode in the period-doubling route to chaos observed for large modulation amplitudes.

IV. POLARIZATION DYNAMICS OF THE MULTIMODE VCSEL SUBJECT TO CURRENT MODULATION

In this section we follow two ways for evaluating the impact of the higher-order transverse mode excitation on the

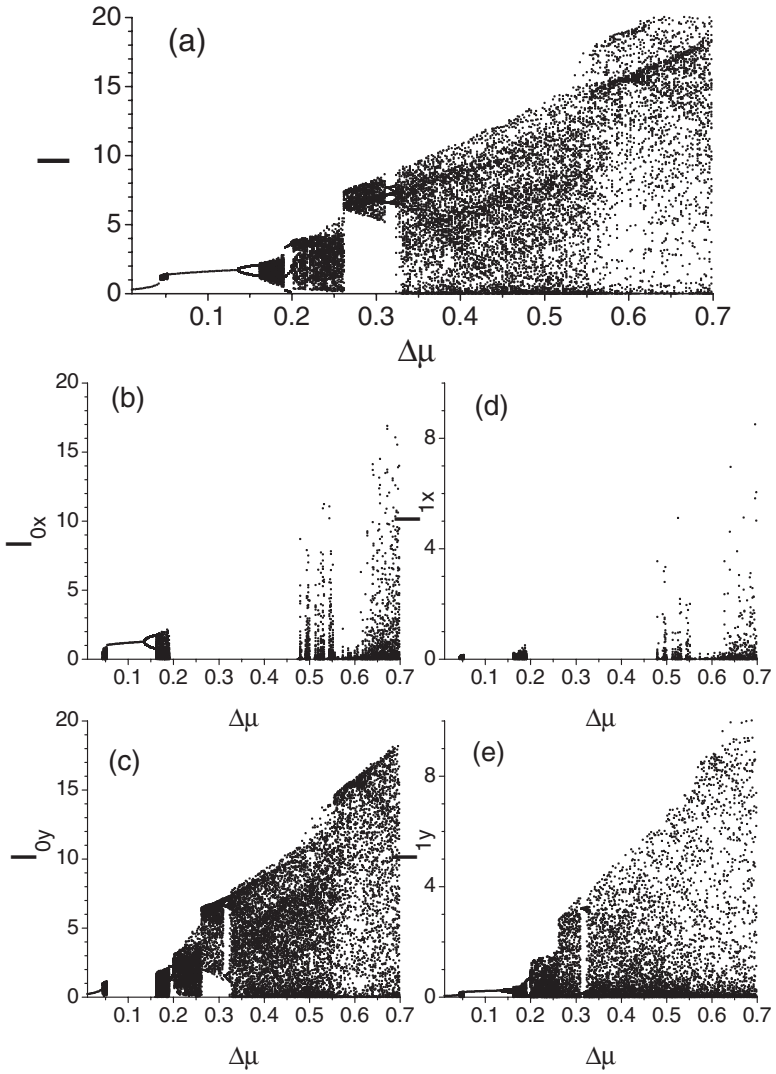

FIG. 4. Bifurcation diagrams of the (a) total, (b) $LP_{01,x}$, (c) $LP_{01,y}$, (d) $LP_{11,x}$, and (e) $LP_{11,y}$ intensities versus $\Delta\mu$, for $s=4$ μm, $F_u=1$ GHz, $\gamma_a=0.1$ ns^{-1}, $\mu_{dc}=1.1$ μ_{th}, and $\kappa_r=1$.

polarization dynamics of the VCSEL. The first one corresponds to considering a VCSEL with a larger area of current injection ($s>a$) in such a way that the higher-order mode is excited for smaller values of the current. The second one corresponds to considering that the loss of the LP_{01} mode is larger than the corresponding to the LP_{11} mode, i.e., $\kappa_r<1$, while maintaining $s=a$. The first situation is illustrated in Fig. 1(b) where the transverse and polarization mode-resolved light-current characteristics of the VCSEL has been plotted when $s=4$ μm. The LP_{11} mode appears at $\mu_{dc}=1.1$ in such a way that for larger values the VCSEL keeps on emitting in both modes. Again, as in Fig. 1(a) the polarization of both transverse modes is the y polarization. The bifurcation diagrams that correspond to this situation are plotted in Fig. 4. We show that periodic and chaotic dynamics are now found for all the polarized transverse modes and for the total intensity. Comparison with Fig. 2 shows that the excitation of the LP_{11} mode, even for small $\Delta\mu$ values, changes the polarization and total intensity dynamics. The main difference is that the LP_{11} mode is now excited with significant power for all the modulation amplitudes. Time-periodic dynamics is now restricted to low values of $\Delta\mu$. The comparison of Figs. 2 and 4 shows that the excitation of the higher-order mode causes indeed a disappearance of the windows of time-periodic regular pulsating dynamics found in the single-mode case for $\Delta\mu>0.32$. We now analyze representative time traces performing a comparison to those found in the

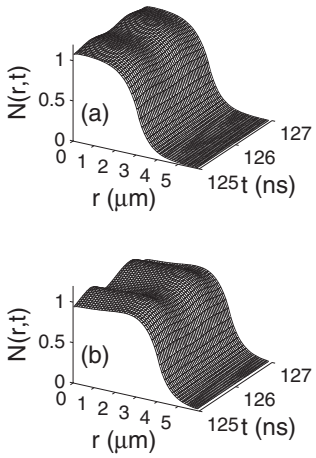

FIG. 5. Temporal evolution of the total carrier number profiles when $\Delta\mu=0.14$, (a) $s=3$ μm, and (b) $s=4$ μm.

single-mode case. We show in Fig. 3(c) a typical time-periodic time trace obtained when $\Delta\mu=0.14$, which is a value slightly above the value where the period-doubling bifurcation occurs (see Fig. 4). A $2T$-periodic response involving the x-polarized fundamental mode and the orthogonal higher-order mode is illustrated in that figure. A comparison between Figs. 3(a) and 3(c) shows that the excitation of the higher-order mode modifies the VCSEL dynamics from a chaotic pulsating dynamics (in the single-transverse-mode case) into a regularly pulsating dynamics (in the two-transverse-mode case). The physical origin of this behavior can be better understood by analyzing the temporal evolution of the corresponding total carrier number profiles. Figures 5(a) and 5(b) show those profiles for the cases corresponding to Figs. 3(a) and 3(c), respectively. In the single-transverse-mode case, Fig. 5(a), the carrier profile always has its maximum at $r=0$ and its shape has only very small changes (the difference between the maximum and minimum value occurs at $r=0$ and is around 0.04). Then both, carrier and mode profiles, remain basically unchanged and the results are similar to those obtained with the spatially independent description. The situation is different for the multitransverse mode case, Fig. 5(b), because the shape of the carrier profile changes along the evolution. When the time is smaller than 125.6 ns the carrier profile is rather flat in such a way that the spatial overlap between the carrier profile and both transverse modes is large. Then modal gains of both transverse modes largely surpass the threshold value and the emitted pulse at around $t=125.6$ ns is basically multimode [see Fig. 3(c)]. Around that emission time the shape of the carrier profile changes, due to the increase in the stimulated recombination of carriers, in such a way that the maximum is now around $r=2.5$ μm. The change of shape of the carrier profile just after the pulse emission is well illustrated in Fig. 5(b) at time=127 ns. The changes in the carrier profile values are larger than for the single-mode case: the difference between the maximum and minimum value of the carriers at $r=0$ is now around 0.15). Those large changes are associated to the period-doubling behavior reported in Fig. 3(c). That period-doubling cannot be obtained with a spatially independent model since it is not able to account for those dynamic changes in the carrier profile. This situation holds for a wide $\Delta\mu$ range ($0.1<\Delta\mu<0.16$). The opposite situation is also found for several $\Delta\mu$ regions. We show in Fig. 3(d) the time traces obtained when $\Delta\mu=0.62$. Trains of pulses of irregular heights appear in the $LP_{01,y}$ and $LP_{11,y}$ modes. Those pulses

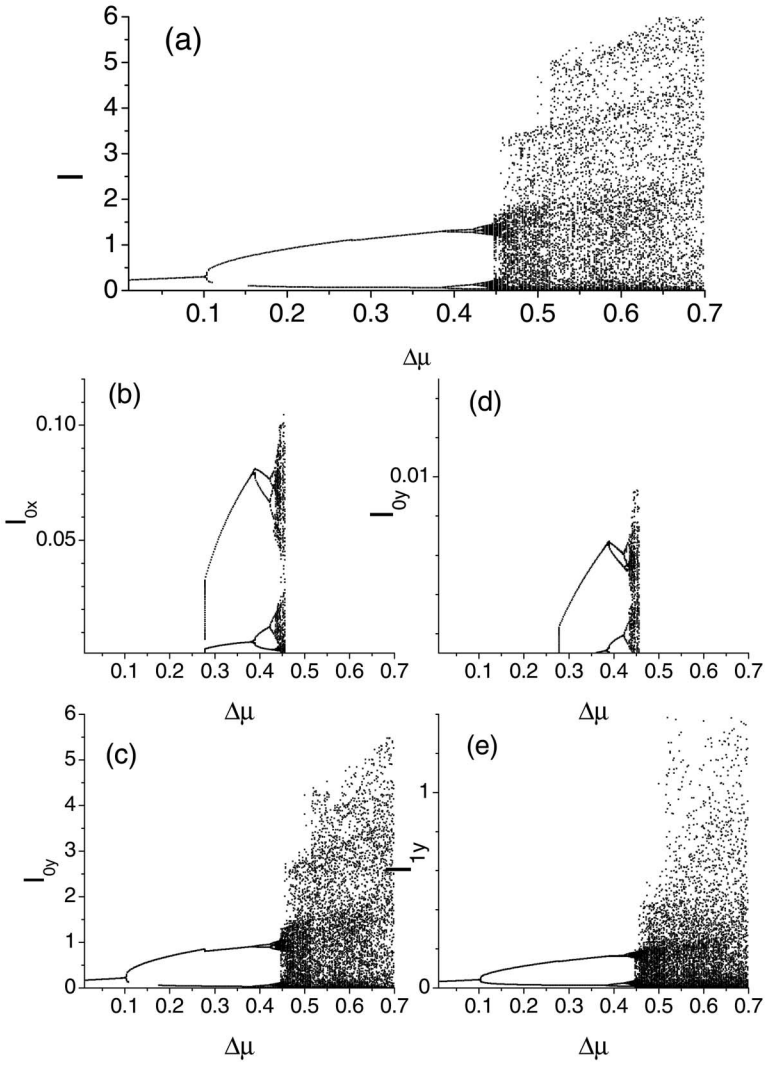

FIG. 6. Bifurcation diagrams of the (a) total, (b) $LP_{01,x}$, (c) $LP_{01,y}$, (d) $LP_{11,x}$, and (e) $LP_{11,y}$ intensities versus $\Delta\mu$, for $s=4$ μm, $F_u=2.5$ GHz, $\gamma_a=0.1$ ns^{-1}, $\mu_{dc}=1.1$ μ_{th}, and $\kappa_r=1$.

appear each $3T$, as in the single-mode operation illustrated in Fig. 3(b), but the height irregularity results in a more complicated dynamics due to the excitation of the higher-order transverse mode. This situation holds for several $\Delta\mu$ intervals ($0.21<\Delta\mu<0.24$, $0.32<\Delta\mu<0.39$, and $\Delta\mu>0.61$). The excitation of the higher-order transverse in such a parameter range therefore modifies the VCSEL dynamics from a regularly pulsating dynamics (in the single-transverse-mode case) into a chaotic pulsating dynamics (in the two-transverse-mode case). We also show in Fig. 3(e) a typical case in which all the polarized transverse modes evolve in a chaotic way. Modulation periods can be found where the four polarized transverse modes are excited with significant power (see, for instance, $80\ \text{ns}\leq t\leq 81\ \text{ns}$, $89\ \text{ns}\leq t\leq 90\ \text{ns}$). The previous results do not depend on the way of achieving multitransverse mode operation because bifurcation diagrams obtained for $s=3$ μm, and $\kappa_r=0.9$ (not shown in this work) are very similar to those shown in Fig. 4.

We now analyze the dependence of the polarization dynamics of the multimode VCSEL on the modulation frequency. We show in Fig. 6 the bifurcation diagrams obtained with the parameters of Fig. 4 but increasing F_u to 2.5 GHz, a value that is approximately twice the relaxation oscillation frequency of the single-mode VCSEL (1.23 GHz) [20]. A period-doubling route to chaos is observed when increasing $\Delta\mu$. The T-periodic solution involves only the y polarization of both transverse modes. That is also the situation for the $2T$ solution while $\Delta\mu$ is smaller than 0.28. For larger $\Delta\mu$ values $2T$-periodic solutions for $\text{LP}_{01,x}$ and $\text{LP}_{11,x}$ modes also appear. All the polarized transverse modes participate with significant power in the period-doubling cascade that leads to the chaotic behavior. As an example of that time-periodic dynamics we show in Fig. 7(a) the temporal evolution of the $4T$ solution that appears when $\Delta\mu=0.41$. Chaotic dynamics involving all polarized transverse modes is only obtained for a narrow $\Delta\mu$ range. We illustrate that dynamics in Fig. 7(b), where the temporal traces of the intensity have been plotted for $\Delta\mu=0.454$. For $\Delta\mu>0.46$, $\text{LP}_{01,x}$ and $\text{LP}_{11,x}$ suddenly drop in such a way that the chaotic dynamics with appreciable power is only observed for the y-polarized transverse modes. We show in Fig. 7(c) an example of that dynamics. The regularity in the time of the emission of the pulses have disappeared in such a way that bursts of closely spaced low-power pulses coexist with well separated higher-power pulses.

We finally present some bifurcation diagrams obtained for several interesting limit cases. The first one is illustrated in Figs. 8(a)–8(c) and corresponds to the case in which only the higher-order mode has significant power. This situation has been achieved by using the parameters of Fig. 2 and by choosing a very small value of the relative losses, $\kappa_r=0.7$. The periodic solutions only appear in the $\text{LP}_{11,y}$ mode. A narrow chaotic window involving only that mode appears around $\Delta\mu=0.43$. The situation changes for larger $\Delta\mu$ because chaos in both polarizations of the higher-order mode is observed when $\Delta\mu>0.455$. The second limit case, shown in Figs. 8(d)–8(f), corresponds to emission in only one linearly polarized mode but with different transverse modes. That emission has been obtained by increasing the value of the dichroism γ_a of Fig. 4 to 0.5 ns^{-1}. A period-doubling route to chaos involving both y-polarized transverse modes is clear from those figures. These results are in agreement with previous reports on chaotic behavior due to the transverse mode competition in VCSELs [18,19].

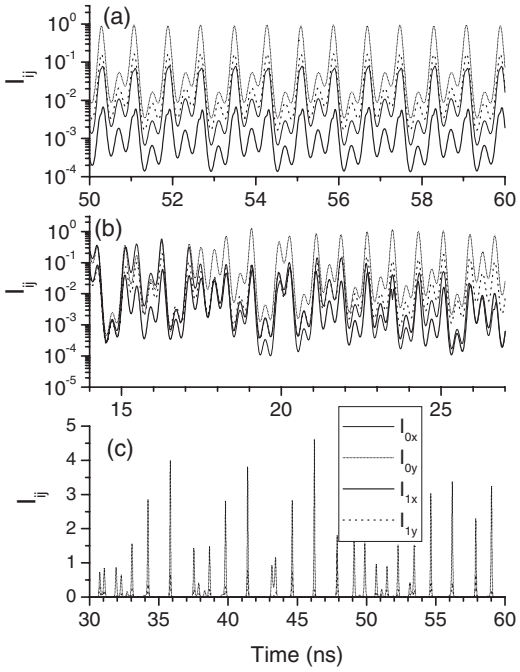

FIG. 7. Time traces of the intensities of the polarized transverse modes for specific values of $\Delta\mu$ (I_{0x}: solid thin line; I_{0y}: dotted thin line; I_{1x}: solid thick line; I_{1y}: dotted thick line). Results correspond to Fig. 5 and are plotted when (a) $\Delta\mu=0.41$, (b) $\Delta\mu=0.454$, and (c) $\Delta\mu=0.6$.

V. DISCUSSION AND CONCLUSIONS

The systematic parameter scannings performed in the previous sections have unveiled several scenarios for the polarization and transverse mode nonlinear dynamics in the VCSEL system with large current modulation: time-periodic, period-doubling, and possibly chaotic dynamics in either one or the two polarization modes of the VCSEL and with fundamental and/or higher-order transverse mode profiles. We now discuss the robustness of the reported nonlinear dynamics against the inclusion of spontaneous emission noise, as it should be done when dealing with realistic VCSEL experiments. The spontaneous emission noise is indeed always present in real devices and can affect the nonlinear dynamics of the polarization of gain-switched VCSELs [20]. We have plotted Figs. 7(a) and 7(b) in logarithmic scale to explicitly show the minimum values of the intensities of the polarized transverse modes. Minimum values are above the 10^{-4} intensity value. For typical values of the spontaneous emission rate ($\beta_{sp}=10^{-5}$ ns^{-1} spontaneous emission rate) the level of the intensity at which the spontaneous emission fluctuations dominate the dynamics is around 10^{-6} [see Fig. 6(d) of Ref. [20]]. Then the reported intensity nonlinear dynamics would remain similar if spontaneous emission fluctuations would have been included in our model. Then it is expected that

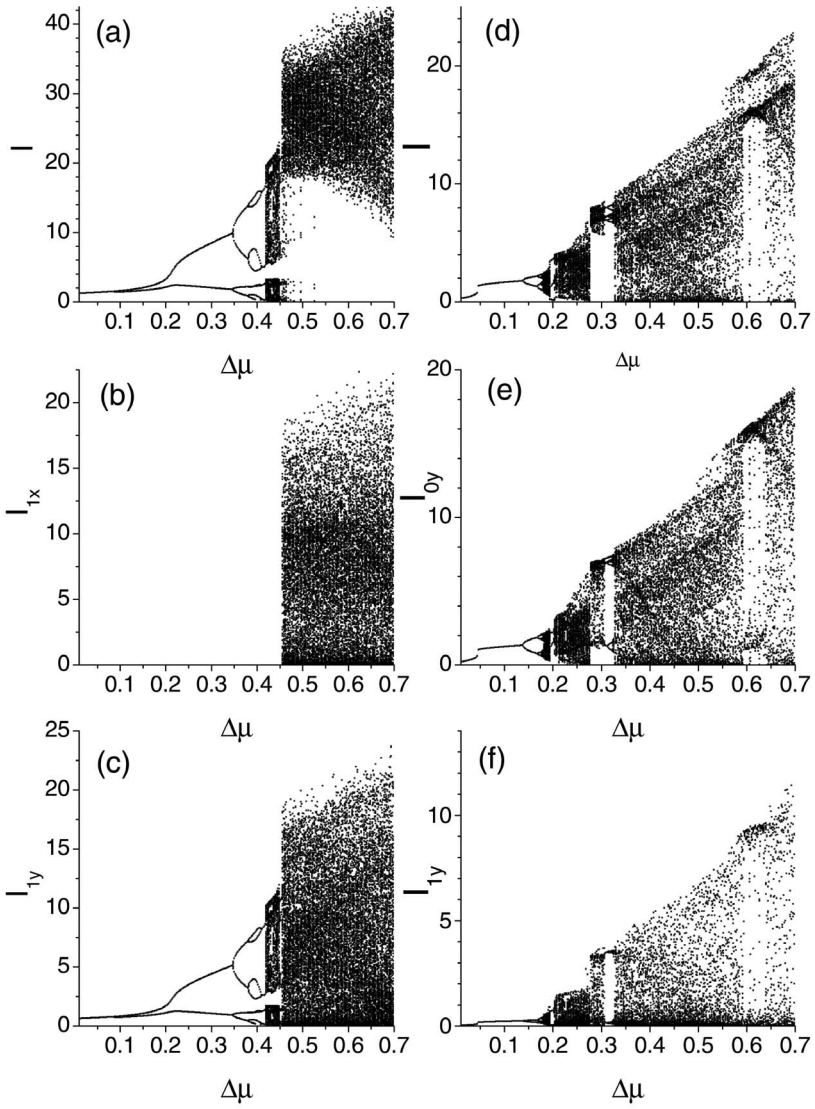

FIG. 8. Left part: bifurcation diagrams of the (a) total, (b) LP11,x, (c) $LP_{11,y}$ intensities power versus $\Delta\mu$, for $s=3$ μm, $\gamma_a=0.1$ ns^{-1}, and $\kappa_r=0.7$. Right part: bifurcation diagrams of the (d) total, (e) $LP_{01,y}$, (f) $LP_{11,y}$ intensities versus $\Delta\mu$, for $s=4$ μm, $\gamma_a=0.5$ ns^{-1}, and $\kappa_r=1$. In this figure $F_u=1$ GHz and $\mu_{dc}=1.1$ μ_{th}.

there would be an appreciable range of the parameters of the system in which nonlinear dynamics similar to the one described in this work would be experimentally observed. This is confirmed by a preliminary experimental work [27] in which the polarization dynamics of a gain-switched single-transverse mode VCSEL has been measured. In that work it is shown that the competition between polarizations induce a loss of regularity in the individual polarizations while the total intensity behaves in a regular way [27]. The simpler problem of the nonlinear dynamics of the gain-switched linearly polarized single-transverse mode VCSEL has only been addressed from a theoretical point of view [17–19]. In those works no chaotic response was obtained. However, we show in Fig. 9 a bifurcation diagram obtained by increasing the value of the modulation frequency and the dichroism of Fig. 2. A period-doubling route to chaos involving only the $LP_{01,y}$ polarized mode is obtained. Similar results were also obtained with the spatially independent model of the single-mode VCSEL with a different set of parameters [26]. Those results indicate that the possibility of achieving chaos in the current modulated linearly polarized single-transverse mode VCSEL remains a question to be addressed.

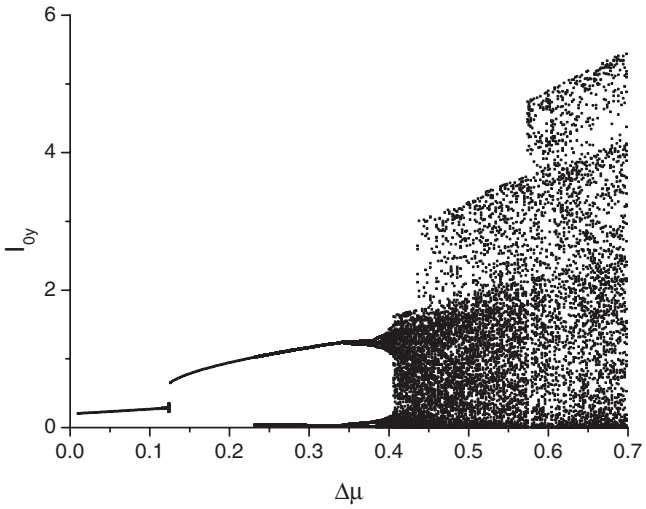

FIG. 9. Bifurcation diagram of the $LP_{01,y}$ intensity versus $\Delta\mu$, for $s=3$ μm, $F_u=2.5$ GHz, $\gamma_a=0.5$ ns^{-1}, $\mu_{dc}=1.1$ μ_{th}, and $\kappa_r=1$. Results are only plotted for the $LP_{01,y}$ mode since the other polarized modes have negligible power.

In this work we have analyzed in a theoretical way the nonlinear dynamics of the polarization of a directly modulated multitransverse VCSEL. Our results have been obtained with a spatially dependent model. We have shown that the spatial effects in a fundamental mode VCSEL modifies the polarization dynamics that accompanies the period-doubling route to chaos for large modulation amplitudes. We have also shown in different parameter regions that the excitation of a higher-order transverse mode may either induce chaotic pulsing in an otherwise regularly pulsating VCSEL, or induce a time-periodic pulsing dynamics in an otherwise chaotic VCSEL. A systematic analysis of bifurcation diagrams for different modulation frequencies, different values of the dichroism, and different transverse mode characteristics allow us to identify the different scenarios of polarization dynamics in directly modulated VCSEL. The reported polarization and transverse mode dynamics are robust when accounting for spontaneous emission noise, hence motivating their experimental observations.

ACKNOWLEDGMENTS

This work was supported in part by the BELSPO IAP 6/10, of FWO-Vlaanderen, and of the OZR-VUB for the GOA and IOF projects, and in part by COST 288 European Action. A.V. acknowledges support from the Ministerio de Educación y Ciencia (MEC) under project No. TEC2006-13887-C05-02/TCM. M.S. acknowledges the support of Conseil Régional de Lorraine.

[1] C. J. Chang-Hasnain, J. P. Harbison, G. Hasnain, A. C. von Lehmen, L. T. Florez, and N. G. Stoffel, IEEE J. Quantum Electron. **27**, 1402 (1991).
[2] D. Vakhshoori, J. D. Wynn, G. J. Zydzik, M. Asom, K. Kojima, R. E. Leibenguth, and R. A. Morgan, Appl. Phys. Lett. **62**, 1448 (1993).
[3] O. Buccafusca, J. L. A. Chilla, J. J. Rocca, S. Feld, C. Wilmsen, V. Morozov, and R. E. Leibenguth, Appl. Phys. Lett. **68**, 590 (1996).
[4] A. Valle, J. Sarma, and K. A. Shore, IEEE J. Quantum Electron. **31**, 1423 (1995).
[5] M. San Miguel, Q. Feng, and J. V. Moloney, Phys. Rev. A **52**, 1728 (1995).
[6] J. M. Martín-Regalado, F. Prati, M. San Miguel, and N. B. Abraham, IEEE J. Quantum Electron. **33**, 765 (1997).
[7] K. D. Choquette, R. P. Schneider, K. L. Lear, and R. E. Leibenguth, IEEE J. Sel. Top. Quantum Electron. **1**, 661 (1995).
[8] K. Panajotov, B. Ryvkin, J. Danckaert, M. Peeters, H. Thienpont, and I. Veretennicoff, IEEE Photonics Technol. Lett. **10**, 6 (1998).
[9] A. Valle, K. A. Shore, and L. Pesquera, J. Lightwave Technol. **14**, 2062 (1996).
[10] B. Ryvkin, K. Panajotov, A. Georgievski, J. Danckaert, M. Peeters, G. Verschaffelt, H. Thienpont, and I. Veretennicoff, J. Opt. Soc. Am. B **16**, 2106 (1999).
[11] C. H. Lee, T. H. Yoon, and S. Y. Shin, Appl. Phys. Lett. **46**, 95 (1985).
[12] Y. C. Chen, H. G. Winful, and J. M. Liu, Appl. Phys. Lett. **47**, 208 (1985).
[13] H. F. Liu and W. F. Ngai, IEEE J. Quantum Electron. **29**, 1668 (1993).
[14] Y. Matsui, S. Kutsuzawa, S. Arahira, Y. Ogawa, and A. Suzuki, IEEE J. Quantum Electron. **34**, 1213 (1998).
[15] H. Lamela, G. Carpintero, and P. Acebo, IEEE J. Quantum Electron. **34**, 1797 (1998).
[16] C. Mayol, R. Toral, C. R. Mirasso, S. I. Turovets, and L. Pesquera, IEEE J. Quantum Electron. **38**, 260 (2002).
[17] S. F. Yu, IEEE J. Quantum Electron. **35**, 332 (1999).
[18] A. Valle, L. Pesquera, S. I. Turovets, and J. M. López, Opt. Commun. **208**, 173 (2002).
[19] J. Y. Law and G. P. Agrawal, Opt. Commun. **138**, 95 (1997).
[20] M. Sciamanna, A. Valle, P. Megret, M. Blondel, and K. Panajotov, Phys. Rev. E **68**, 016207 (2003).
[21] K. Iga, IEEE J. Sel. Top. Quantum Electron. **6**, 1201 (2000).
[22] J. M. Martín-Regalado, S. Balle, M. San Miguel, A. Valle, and L. Pesquera, Quantum Semiclassic. Opt. **9**, 713 (1997).
[23] M. S. Torre, A. Valle, and L. Pesquera, Opt. Quantum Electron. **38**, 445 (2006).
[24] A. Valle, I. Gatare, K. Panajotov, and M. Sciamanna, IEEE J. Quantum Electron. **42**, 322 (2007).
[25] J. Mulet and S. Balle, Phys. Rev. A **66**, 053802 (2002).
[26] M. Sciamanna, A. Valle, K. Panajotov, P. Megret, and M. Blondel, in *Physics and simulation of optoelectronic devices XI*, edited by M. Osinski, H. Amano, and P. Blood, Proceeding of SPIE (SPIE, Washington, D.C., 2003), Vol. 4986, p. 273.
[27] A. Valle, M. Sciamanna, and K. Panajotov, *Physics and Applications of Semiconductor Lasers*, PHASE workshop Technical Digest, 35 (Supelec, Metz, France, 2007).